Gas-Phase Reactions and Rearrangements of Alkyl Esters with H 3 O + , NO + , and O 2 •+ : A Selected Ion Flow Tube Study

ARTICLE *in* THE JOURNAL OF PHYSICAL CHEMISTRY A · NOVEMBER 2007

Impact Factor: 2.69 · DOI: 10.1021/jp0731304 · Source: PubMed

3 AUTHORS, INCLUDING:

Murray Mcewan
University of Canterbury
186 PUBLICATIONS **3,367** CITATIONS

Gas-Phase Reactions and Rearrangements of Alkyl Esters with H_3O^+, NO^+, and $O_2^{\bullet+}$: A Selected Ion Flow Tube Study

Gregory J. Francis,[†,‡] Daniel B. Milligan,[†,‡] and Murray J. McEwan*[,†,‡]

Syft Technologies Ltd., P.O. Box 28149, Christchurch, New Zealand, and Department of Chemistry, University of Canterbury, P.B. 4800 Christchurch, New Zealand

Received: April 23, 2007; In Final Form: July 17, 2007

Selected ion flow tube mass spectrometry (SIFT−MS) has been employed to study the ion−molecule reactions of 17 alkyl esters reacting with the common SIFT−MS reagent ions, H_3O^+, $H_3O^+{\cdot}nH_2O$ ($n = 1, 2, 3$), NO^+, and O_2^+. The majority of reactions were observed to proceed at or near collision rate, with the exception of $H_3O^+{\cdot}3H_2O$, which was found to be slow for 8 of 17 alkyl esters. Unexpected product ions in the form of the parent carboxylic acid cation were observed to arise from the H_3O^+ and NO^+ reactions of some alkyl esters. The observed reactions have been probed by the ab initio CBS-4M and G2(MP2,SVP) methods. The postulated reaction pathway involves a 1,5 H atom migration from a β-carbon onto the carbonyl oxygen.

Introduction

Selected ion flow tube mass spectrometry (SIFT−MS) is an analytical technique based on the ion−molecule chemistry taking place in a flow tube reactor. First introduced by Smith and Spanel,[1] SIFT−MS is now an established technique that has advantages over many other analytical approaches. SIFT−MS provides a quantitative measure of analytes in air mixtures in real time at sensitivities in the low parts per billion level for most analytes,[2] and more recently the parts per trillion level for particular analytes.[3] This very low level quantitation is enabled by a thorough understanding of the chemical kinetics of an analyte with each of the SIFT−MS reagent ions (usually H_3O^+, NO^+, and O_2^+).[1,4] To properly utilize SIFT−MS as an analytical technique, at a level that will provide analyte quantitation, requires knowledge of the rate coefficients, product ion channels and their respective branching ratios, reactions of the water cluster ions with the analyte, and secondary reactions of major product ions with H_2O. Currently, the database of this knowledge contains over 400 compounds which can be quantified by SIFT−MS. The known compounds allow the SIFT−MS instrument to be used in such applications as breath analysis,[1,5] environmental monitoring,[6] oil exploration,[7] and the detection of peroxide based explosives favored by some terrorists.[8] Smith, Spanel, and co-workers[2] have made a determined effort to provide these data for some of the more common analytes. However, there is a need for the addition of many more compounds which are of interest to other applications.

Alkyl esters are common volatile organic compounds due to their relatively high vapor pressure compared to their parent carboxylic acid.[9] Esters are known to have a distinctive odor commonly associated with various fruits, and are often used as artificial flavors or fragrances. For example, isobutyl acetate is a component of banana odor, and along with two other similar esters, makes up 50% of natural banana flavors and smells.[10] The same ester is commonly used as a synthetic replacement for cherry, raspberry, and strawberry flavors. However, the majority of synthesized isobutyl acetate is used as a solvent in artificial cellulose, while only a small percentage is consumed as flavorings and fragrances.

SIFT−MS is an ideal technique for all of these applications due to its rapid screening ability, low limit of detection, and wide quantitation range (parts per trillion up to parts per million).[3]

Experimental Section

The instrument used in the current study is a Voice100 SIFT−MS (Syft Technologies, Christchurch, New Zealand) analytical instrument (Figure 1), which is a small, commercialized, selected ion flow tube mass spectrometer (SIFT−MS). The Voice100 has been briefly mentioned in earlier papers;[3,8] however, it shall be discussed here in substantial detail in relation to the current study. The Voice100 instrument is similar to SIFT−MS instruments described previously by Smith and Spanel,[2] this group,[11] and Schoon et al.[12] with a few subtle, yet important differences.

In the Voice100, ions are generated by a microwave discharge acting on and ionizing a saturated air/water mixture at ~0.3 Torr, a process commonly known as a static afterglow. Reagent ions (H_3O^+, NO^+, and O_2^+) are individually mass selected in the upstream chamber (at $\sim 1 \times 10^{-5}$ Torr) by a quadrupole mass filter, and injected against the pressure gradient into the flow tube through a venturi orifice.

Neutral analyte is introduced into the flow tube at a distance of 6 cm from the venturi, where the carrier gas flow is assumed to be laminar. Ion/molecule reactions are then carried out in the reaction region, which is approximately 25 cm long, with a measured ion transit time of 4 ms. Ions are then sampled through an electrostatic orifice at the end of the flow tube, into the downstream chamber. On entering the downstream chamber (at $< 1 \times 10^{-5}$ Torr), ions resulting from the ion/molecule reaction of interest are mass selected by a second quadrupole mass spectrometer, and detected on a continuous dynode electron multiplier.

The flow tube is approximately 30 cm long and 5 cm in diameter and is bent through 180°, so as to stack the downstream on the upstream chamber, and therefore minimize the overall

[†] Syft Technologies Ltd..
[‡] University of Canterbury.

10.1021/jp0731304 CCC: $37.00
Published on Web 00/00/0000

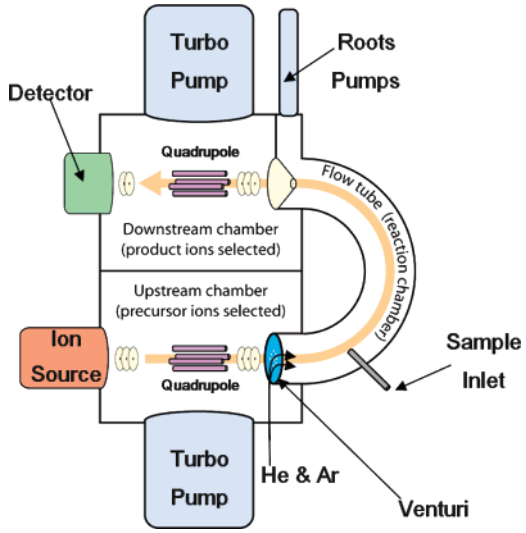

Figure 1. A schematic diagram of the Voice100 SIFT−MS instrument.

footprint of the instrument. Both the upstream and the downstream chambers are pumped by 500 L s^{-1} turbo-molecular pumps, and flow tube gases are removed by a roots blower (100 L s^{-1} at 0.5 Torr). The venturi orifice used on a Voice100 is a dual inlet system, where helium is used to create the venturi effect on an inner annulus, and argon is added through a second annulus on the venturi plate that is further from the center. Argon is employed in the flow tube to decrease radial diffusion, leading to an increased ion density at the sampling orifice, and therefore an increased overall instrument sensitivity when used in the analytical mode.[13] All experiments were performed with a flow tube pressure of 0.5 Torr, and an argon/helium ratio of approximately 3:2. An empirical ion time-of-flight has been measured on the Voice100, which is found to be ~1.6 times faster than the bulk carrier gas velocity. This ratio, and the fact the Reynold's number is less than 100, is indicative of the carrier gas having a laminar velocity profile.[14]

Rate coefficients and branching ratios were determined in the usual way for flow tube kinetics, by the semilogarithmic plot of ion intensity against neutral flow.[15] Appropriate corrections have been included for the differences in diffusion coefficients and also mass discrimination. All esters used in this study were obtained from commercial sources with stated purities of better than 99% in most cases. In the current study, the rate coefficients have been determined absolutely by directly measuring the flow of alkyl ester vapor, which has been purified by freeze−pump−thaw cycling. An example of a typical measurement is given as Figure 2. The uncertainty of the H_3O^+, NO^+, and O_2^+ empirical rate coefficients is deemed to be ±15% based on the addition of uncertainties from each individual piece of experimental equipment used in measuring a rate coefficient, and the accuracy of the linear fit of the semilogarithmic plot. Branching ratios are deemed to have ±30% uncertainty, again based on experimental apparatus, but also based on the extrapolation procedure to determine the branching ratio without interferences from secondary chemistry.

The ion chemistry of H_3O^+ (but not NO^+ or O_2^+) with the esters of this study suffers the complication of water ion cluster formation and some deconvolution of the water ion cluster reactions is necessary to fully understand the H_3O^+ chemistry. We discuss this next. In the presence of mixtures containing water, the water cluster ions at *m*/*z* 37, 55, and 73 are formed. These hydronium ion water clusters ($H_3O^+ \cdot H_2O$ *m*/*z* 37, $H_3O^+ \cdot 2H_2O$ *m*/*z* 55, and $H_3O^+ \cdot 3H_2O$ *m*/*z* 73) cannot be selectively injected into the Voice100 flow tube, as ion declustering occurs on injection. Therefore the rate coefficients of hydronium ion water clusters reacting with the alkyl esters were measured by injecting a small flow of a saturated air/water mixture into the flow tube upstream of the reactant inlet enough to create an appreciable *m*/*z* 73 signal, and then varying the neutral analyte flow. It is important to note that the formation of water clusters occurs throughout the length of the flow tube as the pseudobimolecular rate coefficients for these processes are slow, even at elevated water concentrations. Therefore, as $H_3O^+ \cdot nH_2O$ ions react with the analyte, there is less $H_3O^+ \cdot (n+1)H_2O$ available to react, and the signal of the higher water cluster is lowered. This is only a problem with the initial kinetics and not a problem when monitoring esters at trace levels. To determine the actual values of the $H_3O^+ \cdot nH_2O$ + analyte rate coefficients, the consecutive reaction sequence of all the reactions had to be deconvoluted, and solved to obtain the individual rate coefficients. First the termolecular rate coefficients measured by Young et al.[16] were used and adjusted to the number density of the Voice100 flow tube.[17] These measurements were used as argon was employed as a third body, and they were made at a temperature (337 K) not greatly different from the current study. The rate laws are given as eqs 1−4, where $\nu(X^+)$ is the rate of reaction of X^+ with H_2O, k_n is the rate coefficient of the given ion with H_2O, k_{An} is the rate coefficient of the given ion with the analyte of interest, and $I(X^+)$ is the intensity of the X^+.

$$\nu(H_3O^+) = -k_1 I(H_3O^+) - k_{A1} I(H_3O^+) \quad (1)$$

$$\nu(H_3O \cdot H_2O^+) = -k_2 I(H_3O^+ \cdot H_2O) - k_{A2} I(H_3O^+ \cdot H_2O) + k_1 I(H_3O^+) \quad (2)$$

$$\nu(H_3O \cdot 2H_2O^+) = -k_3 I(H_3O^+ \cdot 2H_2O) - k_{A3} I(H_3O^+ \cdot 2H_2O) + k_2 I(H_3O^+ \cdot H_2O) \quad (3)$$

$$\nu(H_3O \cdot 3H_2O^+) = -k_{A4} I(H_3O^+ \cdot 3H_2O) + k_3 I(H_3O^+ \cdot 2H_2O) \quad (4)$$

Quite complex analytical solutions to the integrated rate laws were determined for each of the $H_3O^+ \cdot nH_2O$ precursor ions; however, a simpler iterative solution was used to deconvolute the rate coefficients in this work. The iterative solution uses an integrated rate law where the individual terms for the above rate expressions are integrated separately. If *t* is the time for each reaction segment then as $t \rightarrow 0$, the iteration solution approximates the flow tube conditions. Therefore, the integrated rate expressions are only evaluated across very short time periods (1/1000 of the total reaction time), and the ion intensity at the end of the flow tube is determined after 1000 iterations. An example of an integrated rate expression applied to the iterative solution for $H_3O^+ \cdot H_2O$ is given as eq 5.

$$I_t^{H_3O^+ \cdot H_2O} = -(I_0^{H_3O^+ \cdot H_2O} \exp(-k_2[H_2O]t)) + (I_0^{H_3O^+ \cdot H_2O} - I_0^{H_3O^+ \cdot H_2O} \exp(-k_{A2}[A]t)) + (I_0^{H_3O^+} - I_0^{H_3O^+} \exp(-k_1[H_2O]t)) \quad (5)$$

$I_t^{H_3O^+ \cdot H_2O}$ represents the ion signal at *m*/*z* 37 at some time *t* corresponding to the iteration time and $I_0^{H_3O^+ \cdot H_2O}$ is the same signal before the iteration. The values of k_{An} are determined by solving using a Newton−Raphson optimization procedure.

The integrated rate expressions (such as eq 5) used for deconvolution of the hydronium ion water cluster rate coefficients require knowledge of the $H_3O^+ \cdot nH_2O + H_2O$ ($n = 0$, 1, 2, 3) rate coefficients. These cannot be measured directly on a Voice100 as $n = 1$, 2, and 3 cluster ions cannot be injected

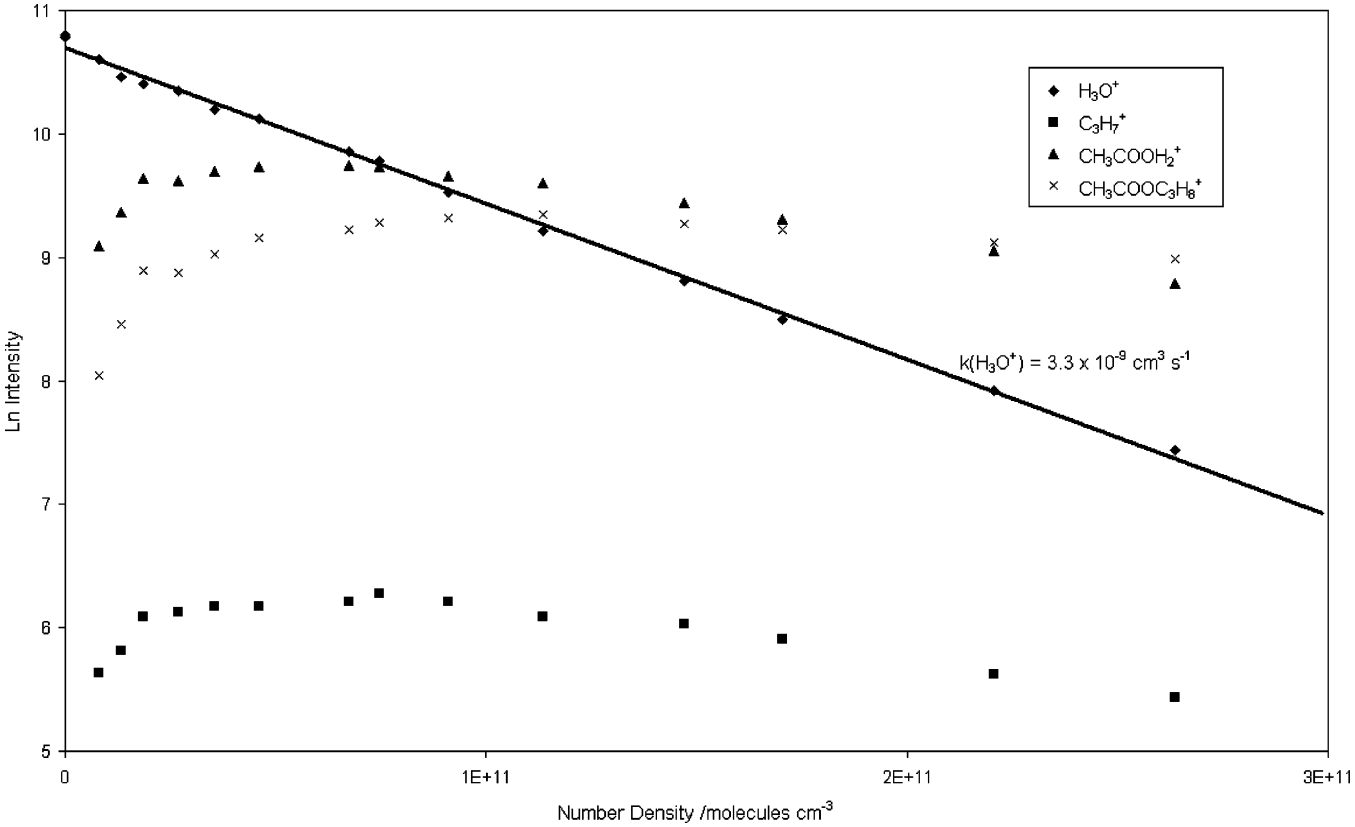

Figure 2. Example of an ion/molecule reaction kinetics plot. H_3O^+ + *n*-propyl acetate ($CH_3COOC_3H_7$).

into the flow tube without collision dissociation breaking up the cluster ion. The termolecular rates are given as eqs 6−8, and are found to predict the $H_3O^+ \cdot nH_2O$ (n = 0, 1, 2, 3) intensities on a Voice100 at a specific humidity. Because these rates predict the observable intensities on a Voice100, the effects of $H_3O^+ \cdot nH_2O$ declustering reactions are minimal. Also the reverse reactions are known to be too slow to influence the results.[18]

			k_3 /cm^6 molecule^{-2} s^{-1}	
$H_3O^+ + H_2O + Ar$	→	$H_3O^+.H_2O + Ar$	6×10^{-28}	(6)
$H_3O^+.H_2O + H_2O + Ar$	→	$H_3O^+.2H_2O + Ar$	6×10^{-28}	(7)
$H_3O^+.2H_2O + H_2O + Ar$	→	$H_3O^+.3H_2O + Ar$	2×10^{-28}	(8)

The accuracy of the measurement of the water clustering rate coefficients is unknown, although it is assumed to be no better than ±30%. But, because the formation of each water cluster is sequential, $H_3O^+ \cdot 2H_2O$ requires two H_2O clustering rates with a cumulative error ±60%, and $H_3O^+ \cdot 3H_2O$ three clustering rates (cumulative error ±90%). As the measurement of hydronium ion water cluster rates requires knowledge of both the $H_3O^+ \cdot nH_2O + H_2O$ clustering rates and the rates of the smaller hydronium ion water clusters with the analyte, the uncertainty on the rate coefficient is large. $H_3O^+ \cdot H_2O$, $H_3O^+ \cdot 2H_2O$, and $H_3O^+ \cdot 3H_2O$ have uncertainties of ±45%, ±90%, and ±135%, respectively.

By reducing the absolute potential applied to the nose-cone sampling orifice at the end of the flow tube to the lowest possible potential in which ion transmission is still acceptable (less than 5 V with respect to ground), collision-induced dissociation of hydronium clusters has been minimized. However, a small amount may still be occurring, which will add to the uncertainties on the rate coefficients given for the hydronium cluster ions and may increase the uncertainty to a value even larger than that quoted here.

TABLE 1: Comparison of Hydronium Ion Water Cluster Rates Measured on Voice100, Using the Iterative Method to Known Literature Rates[a]

	k_{exp} [k_c]/10^{-9} cm^3 s^{-1}			
compound	H_3O^+	$H_3O^+ \cdot H_2O$	$H_3O^+ \cdot 2H_2O$	$H_3O^+ \cdot 3H_3O$
acetone (this study)	3.9 [3.9]	2.7 [3.1]	3.7 [2.8]	2.3 [2.6]
acetone (ref 19)	3.8 [3.9]	3.2 [3.1]	2.8 [2.8]	2.4 [2.6]
acetone (ref 20)		2.3 [3.1]	2.2 [2.8]	2.1 [2.6]
methanol (this study)	2.7 [2.7]	2.3 [2.3]	3.3 [2.1]	0.8 [2.0]
methanol (ref 20)	2.7 [2.7]	1.9 [2.2]	1.8 [2.1]	1.7 [2.0]

[a] All values of k_{exp} measured at approximately 298 K and 0.5 Torr. The collision-limiting rate coefficients are given in parentheses.

The iterative method has been verified against empirical rates of hydronium ion water clusters reacting with acetone as measured by Yang et al.[19] and the rates of the same ions reacting with acetone and methanol as measured by Viggiano et al.[20] are compared in Table 1. The differences in the $H_3O^+ \cdot 2H_2O$ and $H_3O^+ \cdot 3H_2O$ rate coefficients measured in this study compared to the literature rate coefficients is indicative of the large uncertainty. However, the iterative method is preferred due to the ease of measurement. From the comparisons shown in Table 1, it is seen that the current method of iteration gives acceptable agreement with the literature, albeit with increasing uncertainty compared to the direct measurements for n = 2 and 3 clusters.

The results shown in Table 2 for the rate coefficients of the listed ester with the water cluster ions are very sensitive to the rate coefficients for water chemistry that were chosen from the literature. The values chosen here from Young et al.[16] gave the best fits for acetone and methanol that have been determined in other laboratories.

Structures and energies of the analytes and some hydrates have been calculated with the Gaussian 03W suite of software[21]

TABLE 2: Kinetic Parameters of 17 Alkyl Esters Reacting with SIFT−MS Reagent Ions Measured at 298 K and 0.5 Torr

			k_{exp} [k_c][b,c]/10^{-9} cm^3 s^{-1}					
compound	μ_D[a]/debye	α[a]/Å^3	H_3O^+	$H_3O^+\cdot H_2O$	$H_3O^+\cdot 2H_2O$	$H_3O^+\cdot 3H_3O$	NO^+	$O_2^{\bullet+}$
n-butyl formate	2.4 [2.03]	10.0	3.0 [3.5]	3.2 [2.8]	1.7 [2.7]	<0.01 [2.3]	1.3 [2.9]	2.2 [2.8]
n-propyl acetate	2.2 [1.78]	10.2	3.3 [3.3]	3.0 [2.4]	3.2 [2.1]	3.2 [2.0]	1.8 [2.7]	2.2 [2.6]
n-butyl acetate	2.2 [1.87]	12.0	2.9 [3.3]	3.4 [2.5]	4.6 [2.2]	1.8 [2.0]	2.0 [2.8]	2.3 [2.7]
isobutyl acetate	2.2 [1.86]	12.0	3.2 [3.3]	3.3 [2.5]	4.1 [2.2]	<0.01 [2.0]	2.2 [2.8]	2.3 [2.7]
sec-butyl acetate	2.2 [1.87]	12.0	3.1 [3.3]	2.1 [2.5]	2.6 [2.2]	1.8 [2.0]	2.1 [2.8]	2.5 [2.7]
tert-butyl acetate	2.1	11.6	3.2 [3.2]	2.2 [2.5]	2.9 [2.1]	1.8 [1.9]	1.8 [2.7]	2.0 [2.6]
methyl propionate[d]	1.8	8.1 [8.97]	2.7 [3.1]	3.0 [2.4]	3.9 [2.1]	0.7 [1.9]	1.5 [2.6]	1.9 [2.5]
ethyl propionate[d]	2.0 [1.74]	9.9 [10.41]	2.9 [2.9]	3.3 [2.2]	4.6 [1.9]	1.3 [1.8]	1.7 [2.4]	2.2 [2.3]
n-propyl propionate	1.9	11.7	3.3 [3.0]	3.7 [2.3]	4.6 [2.0]	<0.01 [1.9]	2.2 [2.5]	2.2 [2.5]
isopropyl propionate	1.9	11.7	3.1 [3.0]	2.8 [2.3]	3.1 [2.0]	<0.01 [1.9]	2.1 [2.5]	2.2 [2.5]
n-butyl propionate	1.9	13.3	2.9 [3.1]	2.9 [2.4]	3.0 [2.1]	1.7 [1.9]	1.8 [2.6]	2.4 [2.5]
tert-butyl propionate	1.9	13.3	3.0 [3.1]	3.6 [2.4]	2.7 [2.1]	<0.01 [1.9]	1.8 [2.6]	2.3 [2.5]
ethyl butyrate	1.8 [1.74]	12.0	3.0 [3.2]	2.9 [2.2]	3.7 [2.1]	<0.01 [1.9]	2.4 [2.7]	2.5 [2.6]
n-propyl butyrate	1.9	13.6	3.2 [3.2]	2.8 [2.4]	3.6 [2.1]	<0.01 [1.9]	2.0 [2.6]	1.8 [2.6]
isopropyl butyrate	1.9	13.6	2.8 [3.2]	1.5 [2.4]	3.4 [2.1]	<0.01 [1.9]	2.2 [2.6]	2.7 [2.6]
n-butyl butyrate	2.0	15.3	3.1 [3.2]	3.6 [2.5]	2.4 [2.1]	1.1 [1.9]	2.2 [2.7]	2.9 [2.6]
isobutyl butyrate	2.0	15.3	2.9 [3.2]	3.2 [2.5]	1.9 [2.1]	1.3 [1.9]	2.0 [2.7]	2.0 [2.6]

[a] Values calculated with the Gaussian 03 suite at the B3LYP level of theory, using the 6-311(+)G(d,p) basis set. Experimental values sourced from the literature are given in square brackets.[29] All literature values shown of the dipole moment are from liquid phase measurements which are known to have a large associated uncertainty. [b] Experimental rate coefficients (k_{exp}) for H_3O^+, NO^+, and O_2^+ are quoted with ±15% error, and collision limiting rates (k_c) with ±20%. The uncertainty on the hydronium ion water cluster rates is discussed in the text. Collision rates were determined by the parametrized trajectory method of Su and Chesnavich.[25] [c] Rate coefficients of $H_3O^+\cdot nH_2O$that appear anomalously large are discussed in the text. [d] Comparable with literature values for H_3O^+, NO^+, and O_2^+ reactions.[30] Polarizability and dipole moments given in ref 30 for methyl and ethyl propionate are based on estimates, and are not deemed to be accurate enough for a direct comparison.

by the CBS-4M (complete basis set extrapolation) compound method of Petersson and co-workers,[22,23] and the G2(MP2,SVP) compound method.[24] The latter is a more time-consuming method, and has been employed for comparison to the CBS-4M method. All values of electronic energy, enthalpy, and free energy are determined at 298.15 K. Where unknown, dipole moments and polarizabilities have been calculated by using the B3LYP level of theory and a 6-311G(d,p) basis set, with diffuse functions added where necessary.

Results

Experimental absolute rate coefficients and collision limiting rate coefficients for the reactions of 17 alkyl esters with common SIFT−MS reagent ions are given as Table 2. Table 3 then lists the observed product ion masses, an estimation of the ionic structure, and the observed branching ratio. Collision rates have been determined by the method of Su and Chesnavich,[25] where the quoted uncertainty of ±20% is derived from an expected uncertainty on the dipole moment and polarizability. Also included in Table 3 are some thermodynamic parameters of interest. Where the values are available, proton affinities and ionization energies have been sourced from the NIST database[26] with uncertainties on the ionization energy of ±0.2 eV and proton affinity of ±3 kJ mol^{-1}.[27,28]

Discussion

The dipole moments determined in this study by quantum chemical methods are found to be approximately 20% higher than the literature values. However, all the literature values of dipole moment shown in Table 2 were determined from liquid phase measurements, and these are known to have a large uncertainty based on association effects. The two literature values of polarizability given in Table 2 are calculated by a parametrized method, but have been compared to previous experimental values and agree to well within the quoted uncertainty. The values of polarizability calculated by quantum chemical methods in this study are found to be ∼10% lower than the literature values. This observation is possibly attributed in this work to the use of a small basis set, and ignoring important conformers so as to minimize calculation time.

For ethyl propionate, literature values of both dipole moment and polarizability are known. When a collision-limiting rate coefficient is calculated with the literature parameters, the values returned are approximately equal to the values determined when using the quantum chemically calculated dipole moment and polarizability. This observation is fortuitous, but allows for reasonable confidence when calculating collision-limiting rate coefficients for all other esters presented here.

Discussion of H_3O^+ Reactions

All 17 reactions with H_3O^+ were observed to proceed at or near the collision-limiting rate, with proton transfer being a major product ion channel for 16 of the 17 reactions studied. When exergonic proton transfer is observed, experience has shown that the experimental reaction rate is expected to be the collision-limiting rate.[31]

For all reactions of H_3O^+ + ester, where the "alkoxy bound" carbon chain is ethyl or longer (e.g., *ethyl* propionate $C_2H_5O-COC_2H_5$), an unexpected primary product ion is observed. The observed product ion mass corresponds to the mass of the protonated parent carboxylic acid (e.g., for ethyl propionate, *m*/*z* 75 is observed, corresponding to protonated propionic acid). These protonated carboxylic acids were found to be a feature of the H_3O^+ + ester reactions as shown in reaction 9.

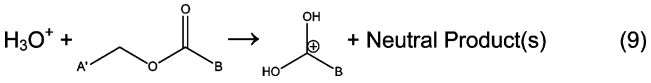

(9)

The formation of a protonated carboxylic acid product ion is supported by Hopkinson et al.,[32] who studied small esters with a variety of reagent ions and supported the data with deuterium labeling studies, and Denekamp and Stanger,[33,34] who studied the collision-induced dissociation of alkyl benzoates. However, the presence of a benzene ring may allow electronic stabilization of some transition states, and the mechanisms proposed by Denekamp and Stanger may not apply to the alkyl esters presented here.

The mechanism of formation of the parent carboxylic acid cation was initially postulated to be similar to a solution-phase

TABLE 3: Product Ions Observed from the Reaction of the Specified Ion with the Ester Listed at 298 K and at 0.5 Torr

				H_3O^+			NO^+			$O_2^{\bullet+}$		
compound	*m*/ g mol^{-1}	PA/ kJ mol^{-1}	IE/ eV	ion	*m/z*	BR	ion	*m/z*	BR	ion	*m/z*	BR
n-butyl formate	102	806.0	10.52	$C_5H_{10}O_2H^+$	103	0.25	$C_5H_{10}O_2{\cdot}NO^+$	132	0.80	$C_5H_{10}O_2^+$	102	0.05
				$C_4H_9^+$	57	0.75	$C_4H_9O^+$	73	0.15	$C_4H_9O^+$	73	0.05
							$C_4H_8^+$	56	0.05	$C_4H_8^+$	56	0.90
n-propyl acetate	102	836.6	9.98	$C_5H_{10}O_2H^+$	103	0.35	$C_5H_{10}O_2{\cdot}NO^+$	132	0.30	$C_3H_5O_2^+$	73	0.10
				$C_5H_9O^+$	85	0.05	$C_5H_9O_2^+$	101	0.20	$C_2H_5O_2^+$	61	0.55
				$C_2H_3O_2H_2^+$	61	0.50	$C_5H_8O^+$	84	0.10	$C_3H_7O^+$	59	0.05
				$CH_3CO^+/C_3H_7^+$	43	0.10	$C_3H_7O^+$	59	0.10	$CH_3CO^+/C_3H_7^+$	43	0.20
							$CH_3CO^+/C_3H_7^+$	43	0.30	$CH_2CO^+/C_3H_6^+$	42	0.10
n-butyl acetate	116		9.94	$C_6H_{12}O_2H^+$	117	0.35	$C_6H_{12}O_2{\cdot}NO^+$	146	0.65	$C_4H_8^+$	56	0.90
				$C_2H_3O_2H_2^+$	61	0.55	$C_6H_{11}O_2^+$	115	0.05	$CH_3CO^+/C_3H_7^+$	43	0.10
				$C_4H_9^+$	57	0.10	$C_4H_9O^+$	73	0.15			
							$CH_3CO^+/C_3H_7^+$	43	0.15			
isobutyl acetate	116		9.97	$C_6H_{12}O_2H^+$	117	0.20	$C_6H_{12}O_2{\cdot}NO^+$	146	0.15	$C_4H_6O_2^+$	86	0.05
				$C_2H_3O_2H_2^+$	61	0.70	$C_6H_{11}O_2^+$	115	0.25	$C_4H_9O^+$	73	0.10
				$C_4H_{10}^+$	58	0.05	$C_4H_6O_2^+$	86	0.05	$C_2H_5O_2^+$	61	0.05
				$CH_3CO^+/C_3H_7^+$	43	0.05	$C_4H_9O^+$	73	0.30	$C_4H_8^+$	56	0.60
							$C_4H_8^+$	56	0.10	$CH_3CO^+/C_3H_7^+$	43	0.20
							$CH_3CO^+/C_3H_7^+$	43	0.15			
sec-butyl acetate	116		9.90	$C_6H_{12}O_2H^+$	117	0.20	$C_6H_{12}O_2{\cdot}NO^+$	146	0.35	$C_6H_{12}O_2^+$	116	0.05
				$C_2H_3O_2H_2^+$	61	0.75	$C_6H_{11}O_2^+$	115	0.05	$C_4H_9O^+$	73	0.05
				$C_4H_9^+$	57	0.05	$C_2H_4O_2{\cdot}NO^+$	90	0.30	$C_2H_5O_2^+$	61	0.30
							$C_4H_8{\cdot}NO^+$	86	0.15	$C_4H_8^+$	56	0.35
							$C_4H_9O^+$	73	0.15	$CH_3CO^+/C_3H_7^+$	43	0.25
tert-butyl acetate	116		10.00[b]	$C_6H_{12}O_2H^+$	117	0.05	$C_6H_{12}O_2{\cdot}NO^+$	146	0.05	$C_5H_9O_2^+$	101	0.30
				$C_4H_9^+$	57	0.95	$C_2H_4O_2{\cdot}NO^+$	90	0.45	$C_2H_3O_2^+$	59	0.10
							$C_4H_8{\cdot}NO^+$	86	0.40	$C_4H_8^+$	56	0.60
							$C_4H_8^+$	56	0.10			
methyl propionate[a]	88	830.2	10.15	$C_4H_8O_2H^+$	89	0.90 (0.95)	$C_4H_8O_2{\cdot}NO^+$	118	0.45 (0.20)	$C_4H_8O_2^+$	88	0.35 (0.25)
				$C_2H_5CO^+$	57	0.10 (0.05)	$C_2H_5CO^+$	57	0.55 (0.80)	$C_2H_5CO^+$	57	0.65 (0.75)
ethyl propionate[a]	102	813.3[b]	10.00	$C_5H_{10}O_2H^+$	103	0.90 (0.95)	$C_5H_{10}O_2{\cdot}NO^+$	132	0.55 (0.60)	$C_5H_{10}O_2^+$	102	0.25 (0.05)
				$C_3H_5O_2H_2^+$	75	0.05	$C_2H_5CO^+$	57	0.45 (0.40)	$C_3H_6O_2^+$	74	0.15 (0.05)
				$C_2H_5CO^+$	57	0.05 (0.05)				$C_2H_5CO^+$	57	0.40 (0.45)
										$C_2H_5O^+$	45	0.20 (0.15)
n-propyl propionate	116		9.96	$C_6H_{12}O_2H^+$	117	0.40	$C_6H_{12}O_2{\cdot}NO^+$	146	0.25	$C_3H_7O_2^+$	75	0.55
				$C_3H\text{-}_5O_2H_2^+$	75	0.40	$C_6H_{12}O_2^+$	116	0.05	$C_3H_5O^+$	57	0.35
				$C_3H_5O^+$	57	0.10	$C_6H_{11}O_2^+$	115	0.10	$C_3H_7^+$	43	0.10
				$C_3H_7^+$	43	0.10	$C_3H_5O^+$	57	0.60			
isopropyl propionate	116			$C_6H_{12}O_2H^+$	117	0.10	$C_6H_{12}O_2{\cdot}NO^+$	146	0.35	$C_5H_9O_2^+$	101	0.05
				$C_3H\text{-}_5O_2H_2^+$	75	0.75	$C_6H_{11}O_2^+$	115	0.40	$C_3H_7O_2^+$	75	0.40
				$C_3H_5O_2^+$	73	0.10	$C_4H_9O_2^+$	89	0.25	$C_3H_5O^+$	57	0.30
				$C_3H_7^+$	43	0.05				$C_2H_5O^+$	45	0.10
										$C_3H_7^+$	43	0.15
n-butyl propionate	130			$C_7H_{14}O_2H^+$	131	0.40	$C_7H_{14}O_2{\cdot}NO^+$	160	0.40	$C_3H_7O_2^+$	75	0.40
				$C_3H_5O_2H_2^+$	75	0.35	$C_7H_{13}O_2^+$	129	0.10	$C_4H_8^+$	56	0.60
				$C_4H_9^+$	57	0.25	$C_4H_8{\cdot}NO^+$	86	0.10			
							$C_4H_9^+$	57	0.40			
tert-butyl propionate	130			$C_7H_{14}O_2H^+$	131	0.10	$C_7H_{14}O_2{\cdot}NO^+$	160	0.05	$C_6H_{11}O_2^+$	115	0.10
				$C_3H_5O_2H_2^+$	75	0.10	$C_3H_6O_2{\cdot}NO^+$	104	0.45	$C_3H_7O_2^+$	75	0.10
				$C_4H_9^+$	57	0.80	$C_4H_8{\cdot}NO^+$	86	0.35	$C_4H_8^+$	56	0.80
							$C_4H_8^+$	56	0.15			
ethyl butyrate	116			$C_6H_{12}O_2H^+$	117	0.80	$C_6H_{12}O_2{\cdot}NO^+$	146	0.30	$C_6H_{12}O_2^+$	116	0.10
				$C_4H_7O^+$	71	0.20	$C_4H_7O^+$	71	0.70	$C_4H_7O^+$	71	0.75
										$C_3H_7^+$	43	0.15
n-propyl butyrate	130			$C_7H_{14}O_2H^+$	131	0.25	$C_7H_{14}O_2{\cdot}NO^+$	160	0.05	$C_4H_9O_2^+$	89	0.60
				$C_4H_7O_2H_2^+$	89	0.30	$C_4H_7O^+$	71	0.85	$C_4H_7O^+$	71	0.30
				$C_4H_7O^+$	71	0.10	$C_3H_7^+$	43	0.10	$C_3H_7^+$	43	0.10
				$C_4H_9^+$	57	0.30						
				$C_3H_7^+$	43	0.05						
isopropyl butyrate	130			$C_4H_7O_2H_2^+$	89	0.45	$C_4H_7O^+$	71	0.30	$C_4H_9O_2^+$	89	0.15
				$C_3H_7O^+$	59	0.25	$C_3H_7O^+$	59	0.65	$C_4H_8O_2^+$	88	0.05
				$C_3H_7^+$	43	0.30	$C_3H_7^+$	43	0.05	$C_4H_7O^+$	71	0.15
										$C_3H_7O^+$	59	0.10
										$C_2H_5O^+$	45	0.35
										$C_3H_7^+$	43	0.20
n-butyl butyrate	144			$C_8H_{16}O_2H^+$	145	0.65	$C_8H_{16}O_2{\cdot}NO^+$	174	0.25	$C_4H_7O^+$	71	0.25
				$C_4H_7O_2H_2^+$	89	0.35	$C_4H_7O^+$	71	0.75	$C_4H_8^+$	56	0.65
										$C_3H_7^+$	43	0.10
isobutyl butyrate	144			$C_8H_{16}O_2H^+$	145	0.20	$C_8H_{16}O_2{\cdot}NO^+$	174	0.35	$C_4H_7O^+$	71	0.40
				$C_4H_7O_2H^+$	89	0.30	$C_8H_{15}O_2^+$	143	0.05	$C_4H_8^+$	56	0.60
				$C_4H_9^+$	57	0.50	$C_4H_7O^+$	71	0.60			

[a] Comparable with literature values.[30] [b] Determined by CBS-4M calculations, using the G03W suite of software. See Table 4.

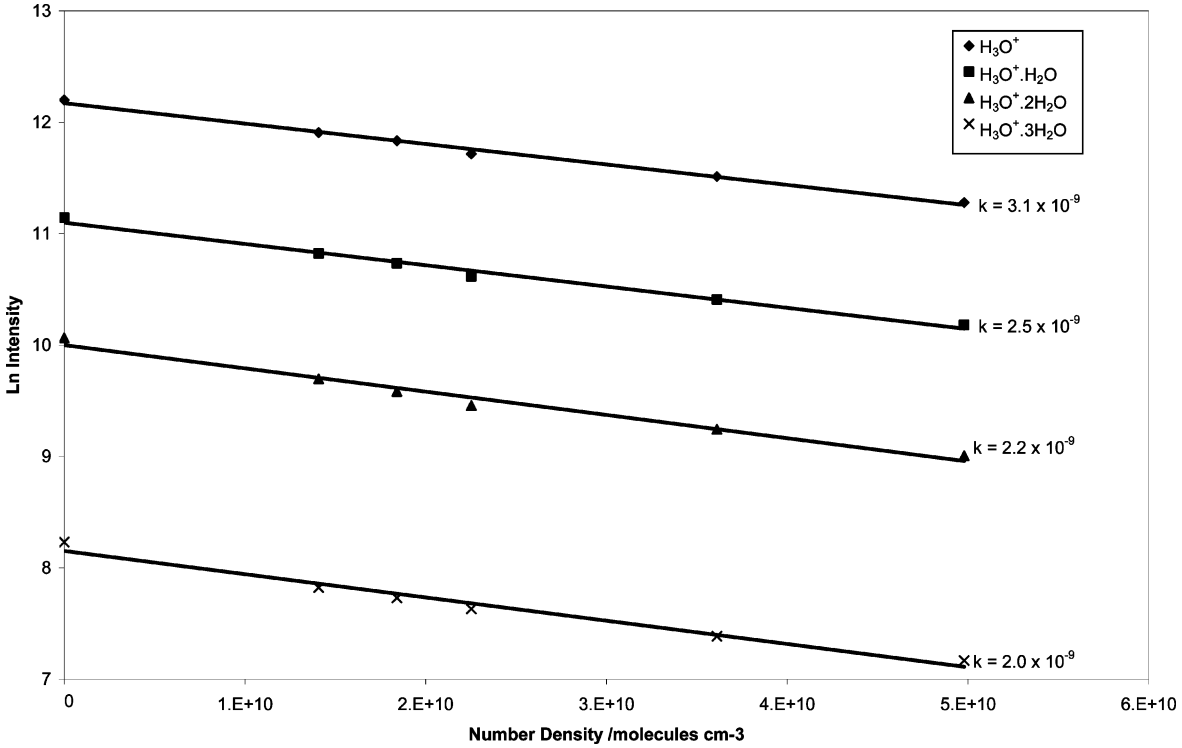

Figure 3. Example of an $H_3O^+ \cdot nH_2O$ ($n = 0, 1, 2, 3$) rate coefficients reacting with neutral analyte. Given values of k have been deconvoluted by the iterative method. The example shown is $H_3O^+ \cdot nH_2O$ + *sec*-butyl acetate ($CH_3COOC_4H_9$).

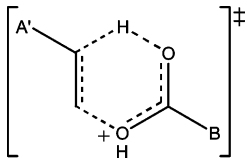

Figure 4. The postulated transition state structure leading to formation of a protonated carboxylic acid.

hydrolysis reaction. In the solution-phase mechanism, H_3O^+ attacks the carbonyl oxygen transferring a proton to this site, then (or simultaneously) a separate water molecule adds to the carbonyl carbon. Following an intramolecular proton migration, the neutral alcohol leaves, and a protonated carboxylic acid group remains. However, a hydrolysis reaction of this nature in the gas phase would require stabilization of the collision complex by a third body (i.e., the reaction would be termolecular), and therefore it is unlikely H_3O^+ "insertion" would be a competitive product ion channel when exergonic proton transfer is also observed, and the reaction is occurring at the collision rate.

The second hypothesis for a mechanism to explain the formation of a protonated carboxylic acid relies on the formation of a six-membered cyclic transition state, where a hydrogen atom migrates from the carbon β to the alkoxy oxygen onto the carbonyl oxygen. This explains the observation that reactions of H_3O^+ with methyl esters (e.g., methyl propionate $CH_3O-COC_2H_5$) do not exhibit carboxylic acid formation as no β-carbon is present. A postulated structure for the transition state is given as Figure 4. Products from such a transition state would be a protonated carboxylic acid and an alkene; therefore, this pathway is reminiscent of a solution-phase cycloreversion mechanism.

The reaction mechanism for the formation of a protonated carboxylic acid parent ion has been probed by using the CBS-4M compound method. Transition state structures were obtained by Synchronous Transit guided Quasi Newton (STQN) methods.[35] Two model chemistry test cases were chosen to study the mechanism: ethyl propionate ($C_2H_5O-COC_2H_5$) and propyl acetate ($C_3H_8O-COCH_3$), two structural isomers with a molecular mass of 102 g mol^{-1}. As shown in Table 3, ethyl propionate was observed to have a 5% channel of m/z 75 (propionic acid, reaction 10), and propyl acetate was observed to have a 50% channel of m/z 61 (acetic acid, reaction 11).

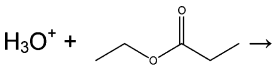

$$C_3H_5O_2H_2^+ \ (m/z = 75) + C_2H_4 + H_2O \qquad 0.05 \qquad (10)$$

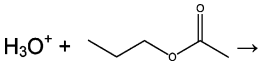

$$C_2H_3O_2H_2^+ \ (m/z = 61) + C_3H_6 + H_2O \qquad 0.50 \qquad (11)$$

As the product ion channel for reaction 10 has a lower branching ratio than the channel for reaction 11, it is hypothesized that the barrier to rearrangement ($\Delta G^{\ddagger}$) is larger for the ethyl propionate reaction 10, than for the propyl acetate reaction 11.

Protonation has been found to be more favorable at the carbonyl oxygen than at the alkoxy oxygen in both cases. The calculated site-dependent proton affinities are given as Table 4.

Table 4 also lists the empirical proton affinity for propyl acetate from the NIST Database (the experimental PA of ethyl propionate is unknown). There is a large discrepancy between the calculated value for protonation at the carbonyl site and the experimental value. The CBS-4M method has a mean absolute deviation for proton affinity on the G2/97 data set of 1.74 kcal mol^{-1} (7.27 kJ mol^{-1}) and a maximum observed error of 3.4 kcal mol^{-1} (14.23 kJ mol^{-1}).[23] The observed uncertainty on the CBS-4M proton affinity of propyl acetate is 23.6 kJ

TABLE 4: Site-Specific Proton Affinity and Gas Basicity at 298 K

		CBS-4M/kJ mol^{-1}		exptl/kJ mol^{-1}	
molecule	protonation site	PA	GB	PA	GB
propyl acetate	carbonyl oxygen	813.0	782.7	836.6[a]	805.6[a]
	alkoxy oxygen	749.5	719.9		
ethyl propionate	carbonyl oxygen	813.3	782.2	unknown	unknown
	alkoxy oxygen	748.3	719.3		

[a] Reference 26.

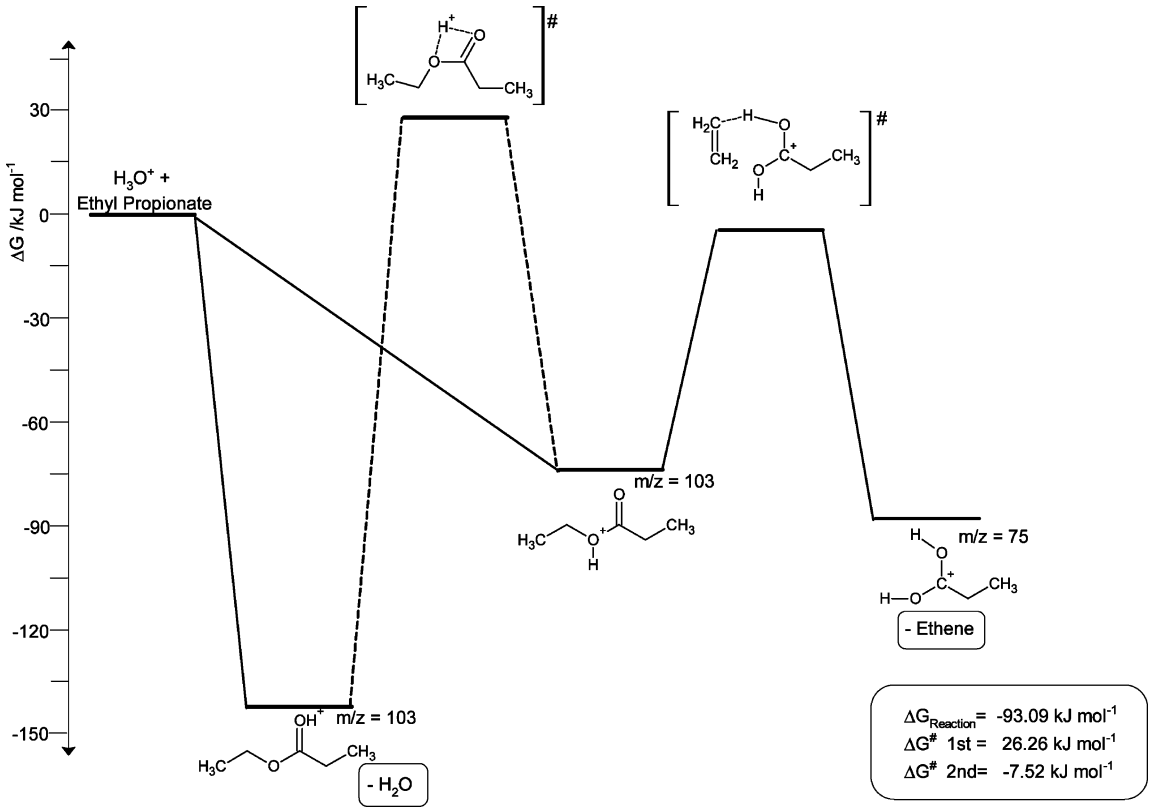

Figure 5. Mechanism of *m/z* 75 formation from protonated ethyl propionate. Initial proton-transfer step from H_3O^+ scaled to the empirical proton affinity/gas basicity of propyl acetate. Free energies determined at 298.15 K.

mol^{-1}, and on the CBS-4M gas basicity it is 22.9 kJ mol^{-1}, which in both cases is substantially larger than the expected error. The CBS-4M method, however, is a very inexpensive multistep "accurate energy" method, and the error is acceptable for a semiquantitative study such as this. CBS-4M energies are therefore assumed to be accurate to within 20−30 kJ mol^{-1}.

Protonation onto the carbonyl oxygen is observed to be a more thermodynamically favorable process than protonation on the alkoxy oxygen (Table 4). However, as both protonation sites are physically close in an ester, the dipole orientation of the neutral molecule approaching H_3O^+ leads to both sites being exposed to protonation. It is therefore expected that protonation will occur at both the carbonyl oxygen and the alkoxy oxygen sites. Where the barrier to 1,3 proton migration is low ($\leq$0 kJ mol^{-1}), the carbonyl oxygen is expected to be the favored site of protonation (thermodynamic control) as rearrangement will be a facile procedure. However, when the barrier to 1,3 proton migration is large, the proton is trapped at a specific site and a statistical distribution of both sites is expected to be observed (kinetic control). Mechanistic potential energy diagrams are given as Figures 5 and 6 for ethyl propionate and propyl acetate, respectively.

Figures 5 and 6 show that the barrier to 1,3 proton migration from the carbonyl oxygen to alkoxy oxygen site is greater than zero in both cases, but a value approximating zero is within the limit of error. Some 1,3 migration will occur due to energy gained from collisions; however, the fraction overcoming the barrier is expected to be low in both the ethyl propionate and propyl acetate cases. The protonation of each ester is therefore approximately under kinetic control. If protonation occurs at the carbonyl oxygen site, the $[M + H]^+$ ion is observed. However, if protonation occurs at the alkoxy oxygen site, the "protonated carboxylic acid" product can be formed. The amount of this acid ion product observed is directly related to the barrier height for 1,5 H atom migration. This barrier is larger in Figure 5 (−7.5 kJ mol^{-1}) than in Figure 6 (−25.2 kJ mol^{-1}), which is consistent with the observed branching ratios of each ester (0.05 and 0.50, respectively). Ethyl propionate is observed to have a 90% channel forming the $[M + H]^+$ ion. Due to the high barrier to 1,5 H atom migration, only a small percentage of ions are likely to overcome this barrier and therefore this 90% channel is expected to consist of some alkoxy oxygen protonated isomer as well as the carbonyl oxygen protonated isomer.

The optimized 6-membered transition state structure is shown as Figure 7 for the propyl acetate case. It is to be noted that the structure is not in a chair- or boat-type conformation but a planar ring, and the alkoxy C−O bond has elongated to 2.79 Å.

To ensure that the HF/3-21G structural optimization used in the CBS-4M method is sufficient for calculating accurate energies for both transition and ground state structures, a step

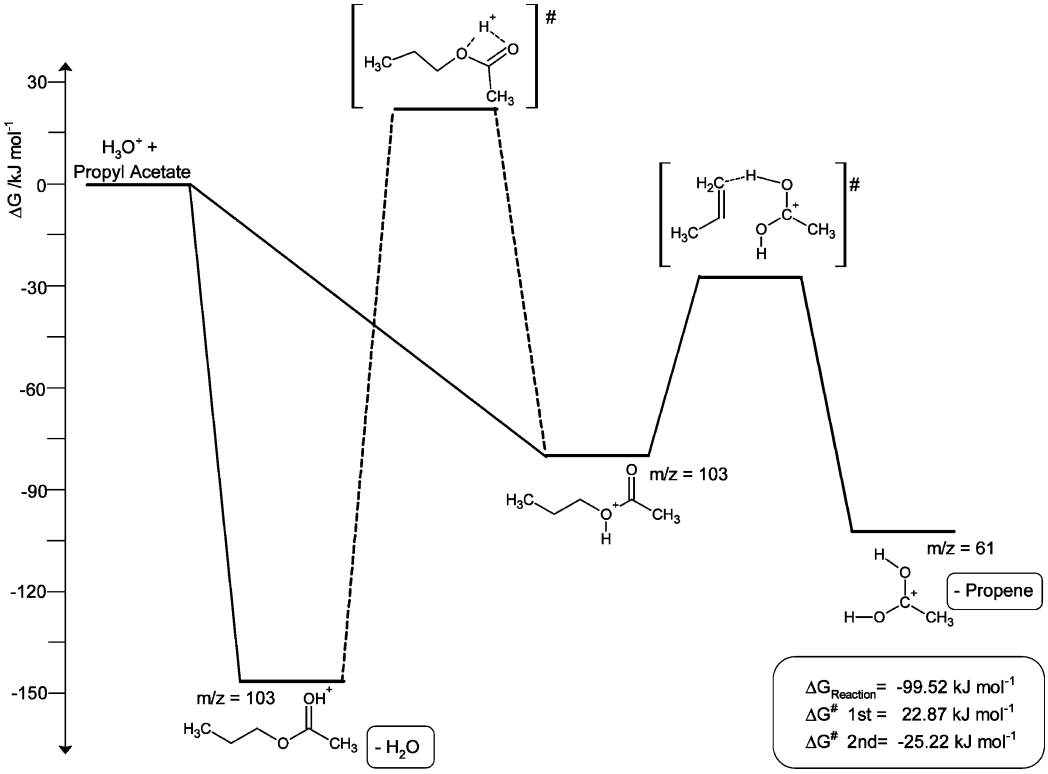

Figure 6. Mechanism of *m*/*z* 61 formation from protonated propyl acetate. The initial proton-transfer step from H_3O^+ corresponds to the empirical proton affinity/gas basicity of propyl acetate. Free energies determined at 298.15 K.

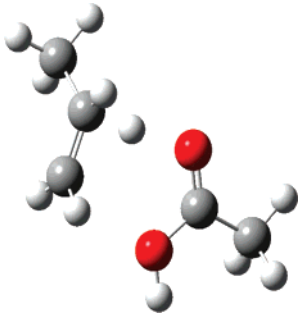

Figure 7. Optimized transition state structure for the 1,5-migration of an H atom in propyl acetate.

of the mechanism shown in Figure 5 has been repeated with the G2(MP2,SVP) accurate energy method. The G2(MP2,SVP) method is much more computationally intensive and therefore is a more expensive accurate energy method, but optimizes structures to the MP2(Full)/6-31G(d) level of theory. Where the CBS-4M method found a barrier of 22.87 kJ mol^{-1} for 1,3-migration, the G2(MP2,SVP) method found a barrier of 27.72 kJ mol^{-1}. The difference of 4.85 kJ mol^{-1} (1.16 kcal mol^{-1}) is well inside the quoted error of both methods with the G2/97 data set. The G2(MP2,SVP) barrier is consistent with the protonation step being under kinetic control.

Aprea et al. observed a similar reaction at the higher ion-neutral interaction energies of PTR-MS.[36] However, Aprea et al. have incorrectly assigned the mechanism as a McLafferty rearrangement, as they have not taken into account the effects of protonation at the alkoxy site.

Discussion of $H_3O^+ \cdot nH_2O$ Reactions (n = 1, 2, 3)

After deconvolution with the algorithm given in the experimental section, the rate coefficients for the water clusters of H_3O^+ reacting with analyte molecules have been calculated.

Because of the large error on each of the termolecular rate coefficients required for deconvolution, rate coefficients given in Table 2 for $H_3O^+ \cdot nH_2O$ (n = 1, 2, 3) are assumed to be only indicative of reaction occurring at the limiting collision rate coefficient, or of no reaction at all. All reactions of $H_3O^+ \cdot H_2O$ and $H_3O^+ \cdot 2H_2O$ are observed to occur with the quoted uncertainty of the collision limiting rate coefficient, and 9 of the 17 reactions of $H_3O^+ \cdot 3H_2O$ are observed to react at or near the collision rate coefficient. The remaining $H_3O^+ \cdot 3H_2O$ rate coefficients are concluded not to react with an appreciable rate coefficient ($< 1 \times 10^{-10}$ cm^3 $molecule^{-1}$ s^{-1}).

Esters studied that have known empirical proton affinities range from approximately 800 to 840 kJ mol^{-1}, and therefore proton transfers from H_3O^+ and $H_3O^+ \cdot H_2O$ to all the measured esters are expected to be exergonic reactions.[31] However, $H_3O^+ \cdot 2H_2O$ and $H_3O^+ \cdot 3H_2O$ are not expected to undergo proton transfer, as this will be an endergonic process. Therefore, any observed reactions of $H_3O^+ \cdot 2H_2O$ and $H_3O^+ \cdot 3H_2O$ are postulated to be via a "metathesis" or ligand switching type reaction that is favored due to a large contribution from entropy. Ligand switching reactions do not always occur at the collision limiting rate, and are affected by flow tube pressure and carrier gas composition. In all reactions of $H_3O^+ \cdot nH_2O$ reacting with an alkyl ester, an $[M \cdot H_3O^+]$ ion is observed; however, it is very difficult to determine if this ion arises from a ligand switching reaction or from H_2O clustering with the protonated analyte. An example of a ligand switching reaction is given as eq 12.

$$H_3O^+ \cdot 3H_2O + C_3H_7COOCH_3 \rightarrow C_3H_7COOCH_3 \cdot H_3O^+ + 3H_2O \quad (12)$$

Discussion of NO^+ and O_2^+ Reactions

NO^+ has been observed to react with the 17 alkyl esters by hydride abstraction $[M - H]^+$, charge transfer $[M]^+$, and

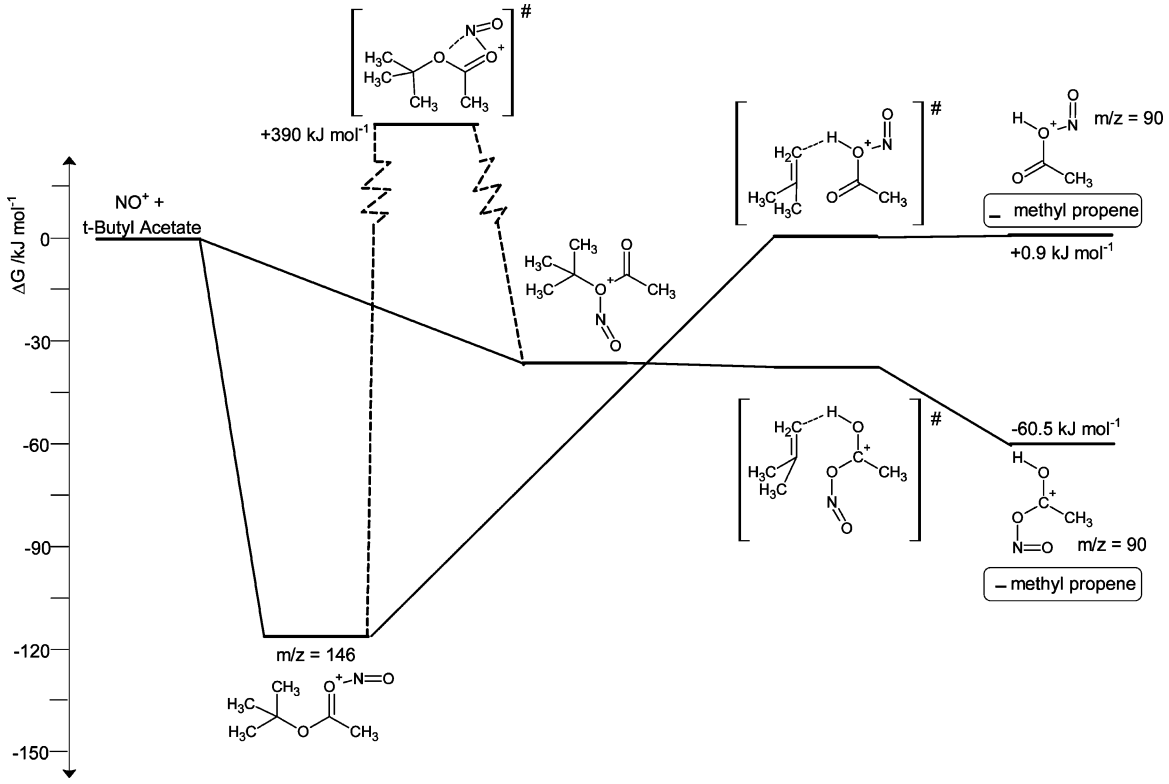

Figure 8. Mechanism of *m*/*z* 90 formation from NO^+ + *tert*-butyl acetate. Free energies were determined at 298.15 K.

association [M·NO^+] pathways with a reaction efficiency of between 50% and 100% of collision rate (reaction efficiency = k/k_c). In addition, some of the studied esters also yield a range of fragment product ions including ions which resemble the carboxylic acid cations observed from H_3O^+ reactions. These product ions are observed when *tert*-butyl propionate ($(CH_3)_3CO(O)CC_2H_5$) (*m*/*z* 130.2) and secondary and *tert*-butyl acetate ($(CH_3)_3CO(O)CCH_3$) (*m*/*z* 116.2) react with NO^+. The structures of these ions are hypothesized to be NO^+-associated carboxylic acid cations. The transition state structure is assumed to be similar to that proposed in Figure 4, with NO^+ replacing the proton. The reaction pathway has also been probed by the CBS-4M method, using *tert*-butyl acetate as a test case, and the lowest calculated energy pathway is shown as Figure 8.

Association of NO^+ at the carbonyl oxygen is more favorable than association at the alkoxy oxygen by 79.9 kJ mol^{-1}. However, the barrier to 1,3 migration of the NO^+ from the carbonyl oxygen to the alkoxy oxygen site is very large (+507 kJ mol^{-1}) and migration will not occur. Therefore, in this case, NO^+ association is completely under kinetic control, and a statistical distribution of association products at both sites will occur. No other NO^+ association sites were found to give a stationary point in the optimization procedure without the presence of one or more negative frequencies.

As can be observed in Figure 8, if association occurs at the carbonyl oxygen, rearrangement to form the [acetic acid·NO^+] product is slightly endergonic (with inclusion of the entropy term) by +0.9 kJ mol^{-1} and may not occur. A 5% [$C_6H_{12}O_2$·NO^+] association channel is observed, and this is totally attributed to association at the carbonyl oxygen site. As the overall reaction efficiency for the reaction of NO^+ and *tert*-butyl acetate is ~0.67, a fraction of associations at the carbonyl oxygen site are assumed to not yield a product ion, and revert to reactants.

When association occurs at the alkoxy oxygen site, there is no barrier to 1,5 H atom migration, and therefore this rearrangement will most likely occur in all cases when NO^+ associates here, i.e., this will be a very facile process. This conclusion is supported by the observation of a large product ion channel at *m*/*z* 90 (45%).

All the measured alkyl esters are assumed to have an ionization energy of less than that of O_2 (12.01 eV) and all are found to proceed by charge transfer to give $[M]^+$ and [M − fragment]$^+$ ions. These fragment ions are complex, and studies into the fragmentation pathways of these ions are continuing.

Conclusions

Because the ester group affords two sites for reaction which are in close proximity (the carbonyl oxygen and the alkoxy oxygen), a range of product ions are formed when alkyl esters undergo cation/molecule reactions. The rearrangement of a protonated alkyl ester to form a parent protonated carboxylic acid has been shown to occur via an intramolecular rearrangement in the gas phase. A similar mechanism holds true when NO^+ associates with a select few alkyl esters to form the [NO^+· carboxylic acid] moiety. The 17 alkyl esters can now be measured quantitatively by using SIFT−MS in the analytical mode. By judicious choice of reagent ion it is also possible to distinguish between some of the isomeric ester pairs.

Acknowledgment. G.J.F. thanks Technology New Zealand for the award of a Ph.D. scholarship. D.B.M. thanks FRST for the award of a postdoctoral fellowship. The authors also acknowledge V. S. Langford, B. J. Prince, and P. F. Wilson for valuable discussions.

Note Added After ASAP Publication. This article was published ASAP on August 28, 2007. Equations 6−8 were missing in that version of the article. The correct version was published September 27, 2007.

References and Notes

(1) Spanel, P.; Smith, D. *Med. Biol. Eng. Comput.* **1996**, *34*, 409−419.

(2) Smith, D.; Spanel, P. *Mass Spectrom. Rev.* **2005**, *24*, 661−700.

(3) Milligan, D. B.; Francis, G. J.; Prince, B. J.; McEwan, M. J. *Anal. Chem.* **2007**, *79*, 2537−2540.

(4) Freeman, C. G.; McEwan, M. J. *Aust. J. Chem.* **2002**, *55*, 491−494.

(5) Wilson, P. F.; Freeman, C. G.; McEwan, M. J.; Milligan, D. B.; Allardyce, R. A.; Shaw, G. M. *Rapid Commun. Mass Spectrom.* **2001**, *15*, 413−417.

(6) Milligan, D. B.; Wilson, P. F.; Freeman, C. G.; McEwan, M. J.; Mautner, M. N.; Clough, T. J.; Sherlock, R. R. *J. Environ. Qual.* **2002**, *31*, 515−524.

(7) Wilson, P. F.; Freeman, C. G.; McEwan, M. J. *Int. J. Mass Spectrom.* **2000**, *229*, 143−149.

(8) Wilson, P. F.; Prince, B. J.; McEwan, M. J. *Anal. Chem.* **2006**, *78*, 575−579.

(9) Vapor Pressure. In *CRC Handbook of Chemistry and Physics*, 86th ed.; Lide, D. R., Ed.; Taylor and Francis: Boca Raton, FL, 2005.

(10) Berger, R.G. In *Volatile Compounds in Foods and Beverages*; Maarse, H., Ed.; Marcel Dekker Inc.: New York, 1991.

(11) Milligan, D. B.; Fairley, D. A.; Freeman, C. G.; McEwan, M. J. *Int. J. Mass Spectrom.* **2000**, *202*, 351−359.

(12) Schoon, N.; Amelynck, C.; Vereecken, L.; Arjis, E. *Int. J. Mass Spectrom.* **2003**, *229*, 231−240.

(13) Francis, G. J.; Milligan, D. B.; Syft Technologies Limited; Improvements in or relating to SIFT-MS instruments; New Zealand Patent Office, N.Z. Patent no. 549242, 2006.

(14) Ferguson, E. E.; Fehsenfeld, F. C; Schmeltekopf, A. L. In *Advances in Atomic and Molecular Physics*; Academic Press: New York, 1969; Vol. 5, pp 1−56.

(15) McEwan, M. J. In *Advance in Gas Phase Ion Chemistry*; Adams, N. G., Babcock, L. M., Eds.; JAI Press: London, UK, 1992; Vol. 1, pp 1−42.

(16) Young, C. E.; Edelson, D.; Falconer, W. E. *J. Chem. Phys.* **1970**, *53*, 4295−4302.

(17) Ikezoe, Y.; Matsuoka, S.; Takebe, M.; Viggiano, A. A. *Gas Phase Ion-Molecule Reactions Rate Constants Through 1986*; Maruzen Comp, Ltd.: Tokyo, Japan, 1987.

(18) Bierbaum, V. M.; Golde, M. F.; Kaufman, F. *J. Chem. Phys.* **1976**, *65*, 2715−2724.

(19) Yang, X.; Zhang, X.; Castleman, A. W., Jr. *Int. J. Mass Spectrom. Ion Proc.* **1991**, *109*, 339−354.

(20) Viggiano, A. A.; Dale, F.; Paulson, J. F. *J. Chem. Phys.* **1988**, *88* (4), 2469−2477.

(21) Frisch, M. J.; Trucks, G. W.; Schlegel, H. B.; Scuseria, G. E.; Robb, M. A.; Cheeseman, J. R.; Montgomery, J. A., Jr.; Vreven, T.; Kudin, K. N.; Burant, J. C.; Millam, J. M.; Iyengar, S. S.; Tomasi, J.; Barone, V.; Mennucci, B.; Cossi, M.; Scalmani, G.; Rega, N.; Petersson, G. A.; Nakatsuji, H.; Hada, M.; Ehara, M.; Toyota, K.; Fukuda, R.; Hasegawa, J.; Ishida, M.; Nakajima, T.; Honda, Y.; Kitao, O.; Nakai, H.; Klene, M.; Li, X.; Knox, J. E.; Hratchian, H. P.; Cross, J. B.; Bakken, V.; Adamo, C.; Jaramillo, J.; Gomperts, R.; Stratmann, R. E.; Yazyev, O.; Austin, A. J.; Cammi, R.; Pomelli, C.; Ochterski, J. W.; Ayala, P. Y.; Morokuma, K.; Voth, G. A.; Salvador, P.; Dannenberg, J. J.; Zakrzewski, V. G.; Dapprich, S.; Daniels, A. D.; Strain, M. C.; Farkas, O.; Malick, D. K.; Rabuck, A. D.; Raghavachari, K.; Foresman, J. B.; Ortiz, J. V.; Cui, Q.; Baboul, A. G.; Clifford, S.; Cioslowski, J.; Stefanov, B. B.; Liu, G.; Liashenko, A.; Piskorz, P.; Komaromi, I.; Martin, R. L.; Fox, D. J.; Keith, T.; Al-Laham, M. A.; Peng, C. Y.; Nanayakkara, A.; Challacombe, M.; Gill, P. M. W.; Johnson, B.; Chen, W.; Wong, M. W.; Gonzalez, C.; Pople, J. A. *Gaussian 03*, Revision C.02; Gaussian, Inc.: Wallingford, CT, 2004.

(22) Ochterski, J. W.; Petersson, G. A.; Montgomery, J. A., Jr. *J. Chem. Phys.* **1994**, *104*, 2598−2619.

(23) Montgomery, J. A., Jr.; Frisch, M. J.; Ochterski, J. W.; Petersson, G. A. *J. Chem. Phys.* **2000**, *112*, 6532−6542.

(24) Curtiss, L. A.; Redfern, P. C.; Smith, B. J.; Radom, L. *J. Chem. Phys.* **1996**, *104*, 5148−5152.

(25) Su, T.; Chesnavich, W. J. *J. Chem. Phys.* **1982**, *76*, 5183−5185.

(26) Hunter, E. P.; Lias, S. G. Proton Affinity Evaluation. In NIST Chemistry WebBook, NIST Standard Reference Database Number 69; Linstrom, P. J., Mallard, W. G., Eds.; National Institute of Standards and Technology, Gaithersburg, MD, June 2005 (http://webbook.nist.gov). Lias, S. G. Ionization Energy Evaluation. In *NIST Chemistry WebBook, NIST Standard Reference Database Number 69*; Linstrom, P. J., Mallard, W. G., Eds.; National Institute of Standards and Technology, Gaithersburg, MD, June 2005 (http://webbook.nist.gov).

(27) Benoit, F. M.; Harrison, A. G. *J. Am. Chem. Soc.* **1977**, *99*, 3980−3984.

(28) Meot-ner (Mautner), M. N. *J. Phys. Chem.* **1980**, *84*, 2716−2723.

(29) Dipole Moments. In CRC Handbook of Chemistry and Physics, 86th ed.; Lide, D. R., Ed.; Taylor and Francis: Boca Raton, FL, 2005. Atomic and Molecular Polarizabilities. In *CRC Handbook of Chemistry and Physics*, 86th ed.; Lide, D. R., Ed.; Taylor and Francis: Boca Raton, FL, 2005.

(30) Spanel, P.; Smith, D. *Int. J. Mass Spectrom. Ion Proc.* **1998**, *172*, 137−147.

(31) Bohme, D. K. The Kinetics and Energetics of Proton Transfer. In *Interactions Between Ions and Molecules*; Ausloos, P., Ed.; NATO Advanced Study Inst. On Ion-Molecule Reactions; Plenum Press: New York, 1975.

(32) Hopkinson, A. C.; Mackay, G. I.; Bohme, D. K. *Can. J. Chem.* **1979**, *57*, 2996−3004.

(33) Denekamp, C.; Stanger, A. *Chem. Commun.* **2002**, 236−237.

(34) Denekamp, C.; Stanger, A. *J. Mass Spectrom.* **2002**, *37*, 336−342.

(35) Peng, C.; Ayala, P. Y.; Schlegel, H. B.; Frisch, M. J. *J. Comput. Chem.* **1996**, *17*, 49−57.

(36) Aprea, E.; Biasioli, F.; Mark, T. D.; Gasperi, F. *Int. J. Mass Spectrom.* **2007**, *262*, 114−121.